Computer Networks 246 (2024) 110407

Contents lists available at ScienceDirect

Computer Networks

journal homepage: www.elsevier.com/locate/comnet

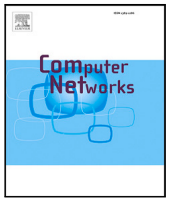

Space-code division multiple access for broadband acoustic networks

Zhengnan Li *, Diego A. Cuji, Milica Stojanovic

Northeastern University, Boston, MA, USA

ARTICLE INFO

Keywords:
SDMA
CDMA
OFDM
Broadband beamforming
Underwater acoustic networks

ABSTRACT

We present an investigation into the design of an acoustic communication network, where multiple users are distributed across space and transmit and receive simultaneously in the same band to and from a common base station. Specifically, we focus on a system that utilizes orthogonal frequency division multiplexing as a modulation method, and allows users to transmit and receive in either synchronous or asynchronous fashion. To distinguish between users on the uplink, the base station employs a combination of code-division and space-division multiple access. The base station iteratively steers a beam to each stable propagation path of the desired user's channel while placing nulls in the direction of other paths, as well as in the directions of interfering users. Finally, the multiple paths of the desired user are recombined before data detection. The process is repeated for each user. Broadband beamforming is employed to account for the broadband nature of acoustic signals. The beamformer coefficients on each carrier depend on the angles of signal arrivals, which are estimated during the uplink transmission and used to construct both the uplink and the downlink beamformer. On the downlink, the base station utilizes angle information to assemble beamforming weights and point in the direction of stable paths of the users. It superimposes multiuser signals and transmits the sum signal to the users. The signal intended for a given user reaches only that user, requiring just a simple detector. Each user is equipped by a single-element transducer. To demonstrate the design concepts, we conducted simulations using a shallow water channel model and performed experimental over-the-air tests in an indoor environment using an acoustic communications testbed. The results were excellent, thereby encouraging future implementations in practical systems.

1. Introduction

Acoustic communications and networking have been extensively studied for underwater channels due to their significance in various oceanographic applications, as well as in the offshore fish farming and oil-and-gas industry [1]. In acoustic networks where multiple users need to transmit to a common base station (BS), a multiple access technique is typically employed, such as time-division or code-division multiple access. While both techniques are capable of distinguishing between multiple users, each user is supported at a transmission rate that is only a fraction of the available bandwidth. Consequently, accommodating more users within a fixed bandwidth leads to a decrease in the per-user rate. Conversely, if the per-user data rate is to be maintained, a bandwidth expansion becomes necessary. However, bandwidth expansion may not be an option in acoustic systems, where bandwidth is naturally scarce.

Space-division multiple access (SDMA) is an alternative technique that eliminates the need for bandwidth expansion by distinguishing between multiple users based on their spatial separation, specifically the different angles from which their signals arrive at the BS. To enable SDMA, the BS must be equipped with a beamforming-capable array, and the users must be spatially separable [2].

Although SDMA has been extensively studied for terrestrial radio applications, demonstrating significant benefits compared to other access methods [2], its exploration in the context of acoustic channels remains limited. At the same time, SDMA presents an ideal solution for overcoming the constraints of limited acoustic bandwidths.

Directive transmission and reception in the forms of beamforming and retrofocusing have been explored by many researchers. Notably, in [3–9], the authors developed and demonstrated the retrofocusing techniques in the form of time reversal. In [6], the authors utilized time reversal to exploit both spatial and temporal diversity to achieve retrofocusing. The authors in [9] experimentally proved the feasibility of a multiple-input multiple-output (MIMO) link, multiplexing up to five data streams. More than 98% of the transmitted single-carrier data blocks were free of bit errors, and the throughput of the system was around 27 kbps.

Beamforming techniques applied to underwater acoustic communications remain scarce [10,11]. In [10], the authors presented a

* Corresponding author.
E-mail address: li.zhengn@northeastern.edu (Z. Li).

https://doi.org/10.1016/j.comnet.2024.110407
Received 21 October 2023; Received in revised form 31 January 2024; Accepted 8 April 2024
Available online 10 April 2024

spatial modulation scheme, aiming at improving the channel capacity and reliability. The proposed methods are corroborated by underwater experiments, demonstrating a nearly 50% greater data rates.

Code-division multiple access (CDMA) has been investigated in both single-carrier and multi-carrier acoustic systems. In Ref. [12], the authors design a spread-spectrum system that adapts to varying channel conditions by adjusting the spreading gain. In [13], the authors evaluate the performance of a spread spectrum multi-carrier system for underwater acoustic communications, utilizing spread spectrum techniques to mitigate ambient noise effects and pre-coding to mitigate multi-user interference. In [14,15], the authors proposed a multi-band spread spectrum design. The entire available bandwidth is divided into subbands, and a single-carrier spread spectrum signal [14], or a multi-carrier signal [15], occupies each subband. In [16], the authors demonstrated the performance of a frequency hopping spread spectrum technique for multi-user communications in experiments.

Directive transmission and reception in the form of beamforming [10,11] and retrofocusing techniques [5,6] have been investigated previously. In [10], the authors presented a spatial modulation scheme, aiming at improving the channel capacity and reliability. The proposed methods are corroborated by underwater experiments, demonstrating a nearly 50% greater capacity. In [6], the authors utilized time reversal to exploit both spatial and temporal diversity to achieve retrofocusing. CDMA has been investigated in both single-carrier and multi-carrier acoustic systems. In Ref. [12], the authors design a spread-spectrum system that adapts to varying channel conditions by adjusting the spreading gain. In [13], the authors evaluate the performance of a spread spectrum multi-carrier system for underwater acoustic communications, utilizing spread spectrum techniques to mitigate ambient noise effects and pre-coding to mitigate multi-user interference.

In this paper, we investigate the design of an acoustic communication network where multiple users, distributed across space, transmit and receive simultaneously and in the same band to and from a common BS. Specifically, we focus on a system in which the users transmit in an asynchronous fashion, employing orthogonal frequency division multiplexing (OFDM) as a modulation method. To distinguish between the users, the BS uses a combination of code-division and space-division multiple access. This design does not require precise time and frequency coordination among users, which, in fact, is infeasible if not impossible in an underwater acoustic network, due to varying propagation delays. The users are expected to transmit in an asynchronous manner, and with the help from both the spreading codes and beamforming, the BS is capable of decoding the superimposed uplink signals. On the downlink, the BS transmit simultaneously to multiple users in the same frequency band, separating the users with different spreading codes and beamforming weights.

To enable code-division, each user is assigned a unique direct sequence (DS) spreading code of length Q, and modulates I information-bearing data symbols onto $K = I \cdot Q$ carriers that comprise one OFDM block. Several OFDM blocks, separated by a cyclic prefix guard interval, are transmitted back-to-back in one frame. The BS is equipped with a uniform linear array, and employs a beamforming strategy that extracts the desired user's signal over a single propagation path, while placing nulls in the directions of multipath components as well as in the directions of interfering users' signals [17]. The process is repeated for all significant paths of the desired user's channel, followed by multipath recombining for extracting an additional gain.

Our previous research focuses on multiuser uplink directive communication, and proposes a broadband beamforming strategy to differentiate between multiple spatially separated users [17]. In [18], we explore the possibility of single user downlink beamforming. Our previous work [19] addressed the design of such a DS-OFDM system where the process of spreading/despreading is coupled with channel estimation needed for coherent detection of phase-shift keying (PSK) or quadrature amplitude modulation (QAM) signals. In particular, the spreading code length Q is chosen to be at least equal to the multipath spread of the channel measured in samples, $L = \lceil BT_{mp} \rceil$, where T_{mp} is the multipath spread and B is the system bandwidth. This choice enables the design of an improved channel estimation method, as well as extraction of the multipath gain. The technique was demonstrated on experimental data, showing good results.

Here, we seek to combine DS-OFDM with front-end beamforming. Our objectives in doing so are twofold: first, to leverage the spatial dimension as an additional means of user separation, and second, to enhance the information throughput. Specifically, we anticipate that the equivalent channel, after beamforming, will exhibit a significantly reduced multipath spread compared to the original channel ($L_{eq} < L$). This reduction enables a decrease in the spreading code length Q, facilitating an increase in the number of information-bearing symbols per block I and therefore enhancing the overall throughput. In an ideal scenario where multipath is fully eliminated, the post-beamforming signal will contain only a single arrival. Consequently, the equivalent channel reduces to a single complex-valued coefficient, ($L_{eq} = 1$), and the choice of Q becomes independent of the multipath spread. This process can be repeated for each path of the desired user's channel, and the multiple paths can subsequently be recombined to achieve additional gains. Likewise, on the downlink, the BS transmits in the direction of the primary path while nulling out all other paths. This design approach minimizes computational requirements for end users while delivering good performance. This article builds on the ideas of [20], and proposes the space-code division multiple access algorithms for downlink scenarios.

The rest of the paper is organized as follows. In Section 2, we introduce the DS-OFDM transmitter design and the channel model, and we overview the angle and delay estimation procedure needed for constructing the beamformer. We then combine DS-OFDM with beamforming, and propose a multipath recombining method that targets an additional multipath gain. In Section 3, we describe the downlink processing, including beamformer design and data detection. In Section 5, we demonstrate the performance of the proposed system in simulation, using a statistical model of a shallow water channel [21]. In addition, we provide experimental results obtained using indoor acoustic transmissions within the Acoustic Communications Testbed (ACT) [21]. Finally, we conclude in Section 7.

2. Uplink

We consider an OFDM system with carrier frequencies $f_k = f_0 + k\Delta f$, $k = 0, \ldots, K-1$, spanning a total bandwidth $B = K\Delta f$. We assume that the system is properly designed such that the duration of one OFDM block, $T = 1/\Delta f$, is much longer than the multipath spread T_{mp}, but short enough to prevent the creation of inter-carrier interference (ICI) due to the time-variation of the channel. We consider a system with an M-element uniform linear array and assume that plane wave propagation holds. The spacing between the array elements, d, is short enough to satisfy the coherence assumption; namely, a signal arriving from direction θ is seen across the array unchanged except for an incremental delay

$$\Delta\tau = \frac{d}{c}\sin\theta \tag{1}$$

where c is the speed of sound.

Following front-end synchronization to the desired user u's signal, Doppler compensation, resampling and fast Fourier transform (FFT) demodulation, the signal observed across the array on carrier k is modeled as

$$\mathbf{y}_{k,u} = a_{k,u}\mathbf{H}_{k,u} + \mathbf{i}_{k,u} + \mathbf{z}_{k,u} \tag{2}$$

where $a_{k,u}$ is the coded data symbol transmitted on carrier k by user u, $\mathbf{H}_{k,u}$ is the channel vector, $\mathbf{i}_{k,u}$ is the multi-user interference term, and $\mathbf{z}_k$ is the noise. Coding is performed such that

$$a_{i+qI,u} = d_{i,u}\delta_{q,u}, i = 0, \ldots, I-1; q = 0, \ldots, Q-1 \tag{3}$$

where $d_{i,u}$ is the information-bearing data symbol coming from a PSK or a QAM alphabet, and $\delta_{q,u}$ is an element (a chip) of the spreading code. In the context of multi-user communications, each user is assigned a unique spreading code.

Assuming that the array elements are spaced closely enough such that they observe the same small-scale fading effects, the channel vector is modeled in terms of the path gains c_p and angles θ_p as

$$\mathbf{H}_{k,u} = \sum_{p=0}^{P-1} c_{p,u} e^{-j2\pi k \Delta f \tau_{p,u}} \underbrace{\begin{bmatrix} 1 \\ e^{-j2\pi f_k \Delta\tau_{p,u}} \\ \vdots \\ e^{-j2\pi f_k (M-1)\Delta\tau_{p,u}} \end{bmatrix}}_{\mathbf{s}_M(f_k \Delta\tau_{p,u})} \tag{4}$$

where P is the number of paths corresponding to the desired user's channel, $\Delta\tau_{p,u} = \frac{d}{c}\sin\theta_{p,u}$, and $\mathbf{s}_M(\cdot)$ is referred to as a steering vector of size M: $\mathbf{s}_M(x) = \begin{bmatrix} 1 & e^{-j2\pi x} & e^{-j2\pi 2x} & \dots & e^{-j2\pi(M-1)x} \end{bmatrix}^\top$.

A beamformer tuned to extracting the signal of path p while nulling out the remaining multipath and interference is characterized by the coefficient vector $\mathbf{w}_{k,p,u}$. Applying this beamformer to the signal $\mathbf{y}_{k,u}$ yields

$$v_{k,p,u} = \mathbf{w}'_{k,p,u}\mathbf{y}_{k,u} = a_{k,u}c_{p,u}e^{-j2\pi k\Delta f\tau_{p,u}} + \xi_{k,p,u} \tag{5}$$

where $\xi_{k,p,u}$ is the residual noise-plus-interference. The beamformer vector $\mathbf{w}_{k,p,u}$ depends on all the angles of arrival (AoA), both those pertaining to the desired user and those pertaining the interfering users. As these angles are not known a-priori, they are estimated and the estimates are used to construct the beamformer. Below, we briefly summarize the angle estimation and beamforming procedure as they will be needed for later interpretation of results.

2.1. Angle estimation

To accurately estimate the angles, the first OFDM block contains all pilots, i.e., all the symbols $a_{k,u}, k = 0, \dots, K-1$, are known to the receiver and are used for AoA estimation. Once the angles have been estimated, the estimates are frozen for the duration of a frame. Such an approach is justified by the fact that unlike the complex gains $c_{p,u}$ or the delays $\tau_{p,u}$, the angles $\theta_{p,u}$ do not change much over a frame in a typical channel geometry, even if the transmitter/receiver pair is moving at a speed of a few meters per second.

We begin by applying a steering operation to the post-FFT signals to obtain

$$x_{k,u}(\theta) = \mathbf{s}'_M(f_k\Delta\tau)\mathbf{y}_{k,u}/a_{k,u}, k = 0, \dots, K-1 \tag{6}$$

We now introduce an additional phase shift to form the metric

$$A_u(\theta,\tau) = \sum_{k=0}^{K-1} x_{k,u}(\theta)e^{j2\pi f_k\tau} = \sum_p c_{p,u}g_{K,M}(\tau-\tau_{p,u}, \Delta\tau-\Delta\tau_{p,u}) + I_u + N_u \tag{7}$$

where I_u stands for the multi-user interference with respect to user u, N_u is the noise, and $g_{K,M}(\tau,\theta)$ is the signature function. This function is defined as

$$g_{K,M}(\tau,\Delta\tau) = \sum_{k=0}^{K-1} g_M(2\pi f_k\Delta\tau)e^{j2\pi k\Delta f\tau} \tag{8}$$

where $g_M(\varphi) = \sum_{m=0}^{M-1} e^{jm\varphi}$. Note that the magnitude $|g_M(\phi)|$ has a pronounced peak at zero, $g_M(0) = M$.

Joint estimation of the channel parameters $c_{p,u}$, $\tau_{p,u}$, and $\theta_{p,u}$ can be performed in an iterative manner over the paths $p = 0, \dots, P-1$, in order of their decreasing strength. In the pth iteration, the estimates of the path delay and angle are obtained as

$$\left(\hat\theta_{p,u}, \hat\tau_{p,u}\right) = \arg\max_{\theta,\tau} \left|A_u^p(\theta,\tau)\right|^2 \tag{9}$$

The corresponding path coefficient is now estimated as

$$\hat c_{p,u} = \frac{1}{KM} A^p(\hat\theta_{p,u}, \hat\tau_{p,u}) \tag{10}$$

and the path's contribution is removed to form a new metric

$$A_u^{p+1}(\theta,\tau) = A_u^p(\theta,\tau) - \hat c_p g_{K,M}(\tau-\hat\tau_{p,u}, \Delta\tau-\hat\Delta\tau_{p,u}) \tag{11}$$

The procedure starts by setting $A_u^0(\theta,\tau) = A_u(\theta,\tau)$ and ends when a pre-set number of paths P has been identified, or when the contribution of the next path falls below a pre-defined threshold. Other aspects, such as ambiguity and resolution properties pertaining to the broadband acoustic array, are discussed in [22].

2.2. Beamformer weights

Taking path p of the user u to be the desired path, the beamformer weights that are associated with the angle $\theta_{p,u}$ (path p of user u) on the kth carrier are denoted by $\mathbf{w}_{k,p,u}$ and are determined so as to ensure that all other paths and all other users are nulled out:

$$\begin{aligned} &\mathbf{w}'_{k,p,u}\mathbf{s}_M(f_k\Delta\tau_{p,u}) = 1, \\ &\mathbf{w}'_{k,p,u}\mathbf{s}_M(f_k\Delta\tau_{q,u}) = 0, \quad \forall q \neq p, \\ &\mathbf{w}'_{k,p,u}\mathbf{s}_M(f_k\Delta\tau_{q,\tilde u}) = 0, \quad \forall q, \forall \tilde u \neq u \end{aligned} \tag{12}$$

Arranging all the steering vectors into a matrix

$$\begin{aligned} \mathbf{S}_k = \Big[&\mathbf{s}_M(f_k\Delta\tau_{0,1}) \dots \mathbf{s}_M(f_k\Delta\tau_{P_1-1,1}) \dots \\ &\mathbf{s}_M(f_k\Delta\tau_{0,U}) \dots \mathbf{s}_M(f_k\Delta\tau_{P_U-1,U}) \Big] \end{aligned} \tag{13}$$

and defining the column vector $\mathbf{e}_{p,u}$ as containing all zeros except for a single 1 at the position corresponding to path p and user u, the beamforming vector associated with path p of user u is compactly defined by

$$\mathbf{w}'_{k,p,u}\mathbf{S}_k = \mathbf{e}'_{p,u} \tag{14}$$

The beamforming vectors that minimize the noise variance are now given by [17]

$$\mathbf{w}_{k,p,u} = \mathbf{S}_k \left(\mathbf{S}'_k\mathbf{S}_k\right)^{-1}\mathbf{e}_{p,u} \tag{15}$$

In a practical implementation, the angles $\theta_{p,u}$ are not known, and their estimates $\hat\theta_{p,u}$ will be used to construct the matrices $\mathbf{S}_k$, i.e. their estimates $\hat{\mathbf{S}}_k$.

2.3. Data detection

Assuming correct operation of the beamformer, the signal at the input to data detection is given by Eq. (5) for a given path p. There can be as many beamformers as there are paths, each producing its own output, or only a single beamformer, tuned to the strongest path. In the former case, multipath contributions can be combined for improved data detection; in the latter, computational complexity will be reduced, possibly still with good detection results.

Collecting the signals $v_{k,p,u}$, defined in Eq. (5), for a given path p over the carriers assigned to the information symbol $d_{i,u}$, and removing the code, we arrange the resulting components into a vector

$$\mathbf{u}_{i,p,u} = \begin{bmatrix} v_{i,p,u}/\delta_{0,u} \\ v_{i+I,p,u}/\delta_{1,u} \\ \vdots \\ v_{i+(Q-1)I,p,u}/\delta_{Q-1,u} \end{bmatrix} = d_{i,u}c_{p,u}e^{-j2\pi i\Delta f\tau_{p,u}}\mathbf{s}_Q(I\Delta f\tau_{p,u}) + \boldsymbol{\xi}_{i,p,u} \tag{16}$$

where $\boldsymbol{\xi}_{i,p,u}$ is the residual noise-plus-interference.

Using the delay estimate obtained from Eq. (9), we now form the signals

$$u_{i,p,u} = \frac{1}{Q}\mathbf{s}'_Q(I\Delta f\hat\tau_{p,u})\mathbf{u}_{i,p,u}e^{j2\pi i\Delta f\hat\tau_{p,u}} \tag{17}$$

If the delay estimate is perfect, these signals will contain as their useful component the terms $d_{i,u}c_{p,u}$, giving rise to a model $u_{i,p,u} = d_{i,u}c_{p,u} + \varepsilon_{i,p,u}$, where $\varepsilon_{i,p,u}$ is a zero-mean residual. Collecting the contributions of different paths into a vector $\mathbf{c}_u = \begin{bmatrix} c_{0,u} & c_{1,u} & \dots \end{bmatrix}^\top$, and forming a

vector $\mathbf{u}_{i,u} = \begin{bmatrix} u_{i,0,u} & u_{i,1,u} & \dots \end{bmatrix}^\top$, the model is equivalently stated as

$$\mathbf{u}_{i,u} = d_{i,u}\mathbf{c}_u + \boldsymbol{\varepsilon}_{i,u} \tag{18}$$

At this point, either coherent or differentially coherent detection can be implemented. While coherent detection requires additional estimation of the path gains $c_{p,u}$, differentially coherent detection does not.

2.3.1. Coherent detection

To estimate the path gains $c_{p,u}$ in coherent detection, a pilot is used to initiate the process. In the simplest approach, the path gains are estimated as

$$\hat{\mathbf{c}}_{0,u} = \mathbf{u}_{0,u}/d_{0,u} \tag{19}$$

where $d_{0,u}$ is a known pilot symbol. These values are used to estimate the remaining information symbols as

$$\hat{d}_{i,u} = \frac{\hat{\mathbf{c}}'_{0,u}\mathbf{u}_{i,u}}{\left\|\hat{\mathbf{c}}_{0,u}\right\|^2}, \quad i = 1, \dots, I-1 \tag{20}$$

Forming the corresponding tentative decision $\tilde{d}_{i,u} = \mathrm{dec}\left\{\hat{d}_{i,u}\right\}$, the channel estimate can be refined using a running average over all current observations,

$$\hat{\mathbf{c}}_{i,u} = \frac{i}{i+1}\hat{\mathbf{c}}_{i-1,u} + \frac{1}{i+1}\mathbf{u}_{i,u}/\tilde{d}_{i,u} \tag{21}$$

If beamforming is not perfect, the equivalent channel will not contain a single path only. Instead, there will be residual multipath components. In such a case, a possible approach is to focus on the beamformer that points to the principal path only, say $p = 0$. The equivalent channel will then consist of L_{eq} taps, spaced by $1/B$. The receiver described in [19] is now applied directly to the observations collected over all carriers, and the processing gain must be kept at least as large as the equivalent channel length, i.e., $Q \le L_{eq}$. However, as mentioned earlier, the equivalent channel length is expected to be significantly shorter than that of the original channel, $L_{eq} \ll L$.

2.3.2. Differentially coherent detection

In differentially coherent detection, the information symbols are differentially encoded such that $d_{i,u} = b_{i,u}d_{i-1,u}$, where $b_{i,u}, i = 1, \dots, I-1$, are the original (uncoded) information symbols, and $d_{i,u}, i = 0, \dots, I-1$ are the differentially encoded information symbols, with $d_{0,u} = 1$. Differentially coherent PSK detection is implemented simply as

$$\hat{b}_{i,u} = \frac{\mathbf{u}'_{i-1,u}\mathbf{u}_{i,u}}{\left\|\mathbf{u}_{i-1,u}\right\|^2} \tag{22}$$

Final decisions are made by finding the nearest constellation points $\tilde{b}_{i,u} = \mathrm{dec}\left\{\hat{b}_{i,u}\right\}$. Note that summing over the paths (inner product in the nominator) extracts the multipath gain; however, the algorithm is equally applicable to a single path. In other words, it is up to the designer to chose the number of paths, i.e., the length of the vector $\mathbf{u}_i$.

3. Downlink

Optimal transmit beamforming requires knowledge of the downlink channel response to all the users. As seen often in the radio literature [2], the uplink and the downlink channels are also assumed reciprocal. These assumptions, however, are not valid in the context of acoustic communication. In fact, the channel can change considerably between the uplink and downlink transmission times, as the low propagation speed of sound (1500 m/s in water) causes long round-trip delays that can make the feedback outdated. The main culprit for the apparent change in the channel response are the phases of the channel coefficients c_p in Eq. (4). These phases contain the contributions of both the small-scale fading and path delays, neither one of which can be predicted with sufficient accuracy to warrant phase alignment on the downlink.

To address this challenge, we propose to beamform only in the direction of the principal path for each user, obviating the need for multipath phase alignment. The beamformer weights thus depend only on the principal path's angle of arrival. While this angle can also vary in time, it does so much more slowly than the overall phase. In fact, it can be assumed nearly invariant in a typical system geometry with a round-trip time of several seconds. For instance, if a mobile acoustic communications user moves at around 1 m/s, its displacement over the time it takes to close the feedback loop over a 1.5 km link will be only 2 m, and the corresponding angle change is negligible.

We denote the $M \times 1$ transmit beamforming vector assigned to user u on the kth carrier by $\mathbf{w}_{k,u}$. The downlink signal transmitted on the mth array element is given by

$$s_u^m(t) = \Re\left\{\sum_{i=0}^{I-1}\sum_{q=0}^{Q-1} d_{i,u}\delta_{q,u}\left(w^m_{i+qI,u}\right)^* e^{j2\pi f_{i+qI}t}\right\}, t \in \left[-T_g, T\right] \tag{23}$$

Downlink can be implemented in a synchronous or an asynchronous manner. In the later case, the signals intended for multiple users are added with pre-defined delays T_u, i.e.,

$$s^m(t) = \sum_{u=1}^{U} s_u^m(t - T_u) \tag{24}$$

The rationale behind this design is that it might help to reduce the peak-to-average ratio in the power of the transmitted signal.

At each user's end, time and frequency synchronization, Doppler compensation and FFT demodulation are performed. The signal after these operations is modeled as

$$y_{k,u} = a_{k,u}\mathbf{w}'_{k,u}\mathbf{H}_{k,u} + \xi_{k,u} \tag{25}$$

where $z_{k,u}$ is the noise, $\xi_{k,u}$ is the noise-plus-interference, and $\mathbf{H}_{k,u}$ is given in (4). Note that the uplink and the downlink channel may not be the same.

Extraction of the path p of user u requires a beamforming vector that maximizes the useful signal power while placing nulls in all other directions:

$$\begin{aligned} &\mathbf{w}_{k,p,u} = \arg\max_{\mathbf{w}} && \left|\mathbf{w}'\mathbf{s}_M(f_k\Delta\tau_{p,u})\right|^2 \\ \text{s.t.c.}\quad &\mathbf{w}_{k,q,u}\mathbf{s}_M(f_k\Delta\tau_{q,u}) = 0, && \forall q \ne p, \forall u \\ &\mathbf{w}_{k,q,\tilde{u}}\mathbf{s}_M(f_k\Delta\tau_{q,\tilde{u}}) = 0, && \forall q, \forall \tilde{u} \ne u \\ &\left\|\mathbf{w}_{k,p,u}\right\|^2 = p_u, && \forall u \end{aligned} \tag{26}$$

where p_u is the per-carrier power allocated to user u (no additional power can be used by increasing the size of the array)

These conditions can be concisely expressed as

$$\mathbf{w}'_{k,p,u}\bar{\mathbf{S}}_{k,p,u} = \mathbf{0}^\top, \forall u \tag{27}$$

where $\bar{\mathbf{S}}_{k,p,u}$ is obtained from $\mathbf{S}_k$ in (13) by removing the column corresponding to path p of user u.

Defining the null space of $\bar{\mathbf{S}}_k$ as

$$\mathbf{N}_{k,p,u} = \mathbf{I} - \bar{\mathbf{S}}_{k,p,u}\left(\bar{\mathbf{S}}'_{k,p,u}\bar{\mathbf{S}}_{k,p,u}\right)^{-1}\bar{\mathbf{S}}'_{k,p,u} \tag{28}$$

the nulling condition (27) is equivalently expressed as [23]

$$\mathbf{N}_{k,p,u}\mathbf{w}_{k,p,u} = \mathbf{w}_{k,p,u} \tag{29}$$

The optimization problem now reduces to finding

$$\begin{aligned} &\max_{\mathbf{w}} \left|\mathbf{w}'\mathbf{N}_{k,p,u}\mathbf{s}_M(f_k\Delta\tau_{p,u})\right|^2 \\ &\text{s.t.c.}\quad \left\|\mathbf{w}_{k,p,u}\right\|^2 = p_u, \forall u \end{aligned} \tag{30}$$

The solution to this problem is given by

$$\mathbf{w}_{k,p,u} = \frac{\sqrt{p_u}}{\sqrt{M_{k,p,u}}}\mathbf{N}_{k,p,u}\mathbf{s}_M(f_k\Delta\tau_{p,u}) \tag{31}$$

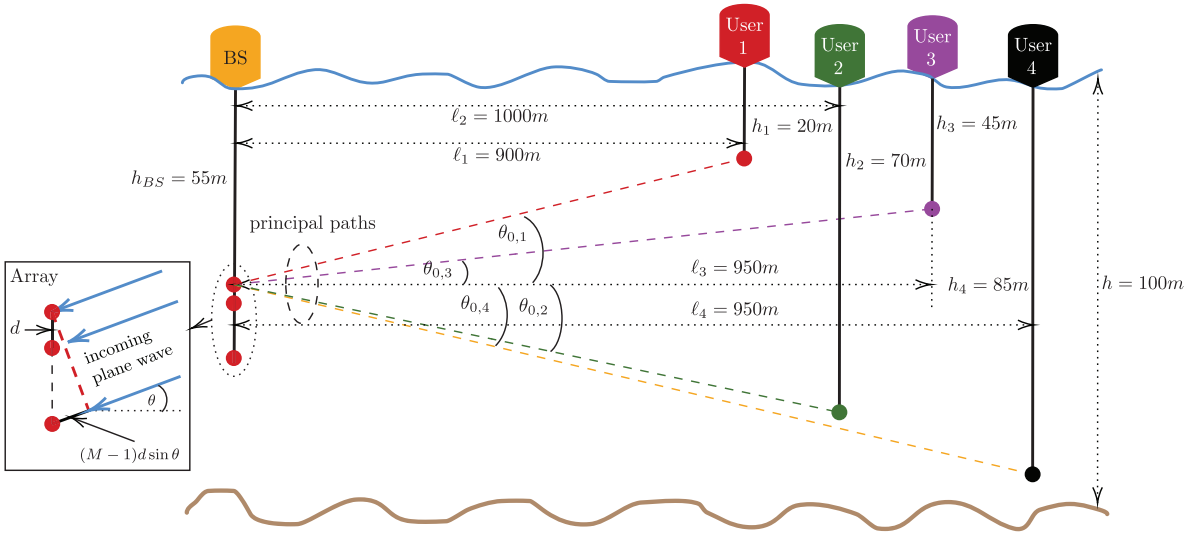

Fig. 1. System geometry.

where

$$M_{k,p,u} = \mathbf{s}'_M(f_k \Delta\tau_{p,u})\mathbf{N}_{k,p,u}\mathbf{s}_M(f_k \Delta\tau_{p,u}) \tag{32}$$

We assume that the paths are completely separable, i.e., $M_{k,p,u} = M$.

If perfect knowledge of the angles is available at the BS, the received signal (25) will contain only the principal path's contribution,

$$y_{k,u} = a_{k,u}\mathbf{w}'_{k,u}\mathbf{H}_{k,u} + \xi_{k,u} = a_{k,u}c_{0,u}e^{-j2\pi k\Delta f \tau_u} + \xi_{k,u} \tag{33}$$

where c_u is the downlink equivalent complex baseband path gain, and $\xi_{k,u}$ is the noise.

Removing the spreading code, and arranging the resulting signals into a vector, we obtain

$$\begin{aligned}\mathbf{u}_{i,u} &= \begin{bmatrix} y_{i,u}/\delta_0 \\ y_{i+I,u}/\delta_{1,u} \\ \vdots \\ y_{i+(Q-1)I,u}/\delta_{Q-1,u} \end{bmatrix} \\ &= d_i c_{0,u} e^{-j2\pi i\Delta f \tau_u}\mathbf{s}_Q(I\Delta f \tau_u) + \mathbf{z}_{i,u}\end{aligned} \tag{34}$$

Note again that the data symbol $d_{i,u}$ is linked to the signal $\mathbf{u}_{i,u}$ by the *same* vector $\mathbf{c}_u$ for each user. From this point, either coherent or differentially coherent detection can be implemented. Differentially coherent detection of the data symbols is performed as

$$b_{i,u} = \frac{\mathbf{u}'_{i-1,u}\mathbf{u}_{i,u}}{\|\mathbf{u}_{i-1,u}\|^2} \tag{35}$$

4. Complexity analysis

The additional complexity of the proposed algorithms are determined by the following three operations, measured in complex number additions and multiplications:

- The joint angle and delay detection, described by Eq. (7). The complexity is $\mathcal{O}\left(|\tau_{obs}| \cdot |\theta_{obs}| \cdot M \cdot K\right)$, where $|\tau_{obs}|$ and $|\theta_{obs}|$ are the number of delay and angle observations, respectively. Such an operation may be repeated P times to iteratively identify the path angles and delays.
- Uplink null-steering beamformer weights calculation, described by Eq. (15). The complexity of this operation is $\mathcal{O}\left(K \cdot U \cdot P^3 \cdot M^2\right)$. The beamformer weights described in Eq. (15) are calculated for each carrier, each path and each user. The pseudo-inverse, if implemented efficiently using singular vector decomposition, has a complexity of $\mathcal{O}\left(M^2 \cdot P\right)$. Finally, the additional multiplication by the nulling vector $\mathbf{e}$ necessitates P complex operations.
- Downlink null-steering beamformer weights calculation, described by Eq. (31). The complexity of this operation is $\mathcal{O}(K \cdot U \cdot P^2 \cdot M^3)$, which includes the nulling operation defined in Eq. (28). Similar to the uplink beamformer complexity, the weights are calculated per carrier, per path and for each user. The complexity of taking the pseudo-inverse of the matrix $\bar{\mathbf{S}}_{k,p,u}$ is $\mathcal{O}(M^2 \cdot P)$. The final multiplication by the steering vector adds additional $\mathcal{O}(M)$ operations.

Note that the DS-OFDM related data detection complexity is negligible when compared to the beamforming algorithms. We refer the reader to [19] for the complexity analysis of the DS-OFDM system.

5. Simulation results

In this section, we assess the performance of the proposed algorithm using a simulated shallow water channel. The system consists of a BS equipped with a vertical array and up to four users ($U \leq 4$), each with a single transmitter/receiver element. The channel geometry (see Fig. 1) is specified by the distances $\ell_1 = 900$ m, $\ell_2 = 1000$ m, $\ell_3 = 950$ m, and $\ell_4 = 950$ m between the array and the users, and depths $h_1 = 20$ m, $h_2 = 70$ m, $h_3 = 45$ m, and $h_4 = 85$ m. The water depth is $h = 100$ m, and the distance between the sea surface and the first receiver element is $h_R = 55$ m. The speed of sound is $c = 1500$ m/s in the water, and 1300 m/s in the bottom, and spherical spreading is assumed on each path. At the time of downlink reception, we assume that the users have drifted at velocity $\mathrm{v}_u \angle \phi_u$; specifically, $\mathrm{v}_1 = 0.5\angle 45°$ m/s, $\mathrm{v}_2 = 0.75\angle 0°$ m/s, $\mathrm{v}_3 = 0.25\angle 90°$ m/s, and $\mathrm{v}_4 = 1\angle -90°$ m/s, such that their distances have changed by $\frac{2d}{c}\mathrm{v}_u \cos\phi_u$, and their depths by $-\frac{2d}{c}\mathrm{v}_u \sin\phi_u$. The element spacing is $d = 0.3$ m, and the number of array elements is $M = 24$. The lowest carrier frequency is $f_0 = 10$ kHz, the bandwidth is $B = 5$ kHz, and the number of carriers is $K = 1024$.

The small-scale fading coefficients are generated according to [21] using the following parameters: standard deviation of the surface height displacement is $\sigma_s = \frac{c}{5f_0}$, standard deviation of the bottom height displacement is $\sigma_b = \frac{c}{3f_0}$, number of micro-paths within one path is $S_p = 20$, mean and variance parameters of micro-path amplitudes are $\mu_{p,0} = 0$, $\mu_p = 1/S_p$, and $\nu_p = \mu_p/10$, respectively. The noise components across the elements are assumed to be i.i.d. zero-mean complex Gaussian, with variance σ^2, and the signal-to-noise ratio (SNR) is defined as $\mathrm{SNR} = \frac{1}{\sigma^2}$. We assume that the users' signals arrive with similar powers (this is possible when each user implements a proper

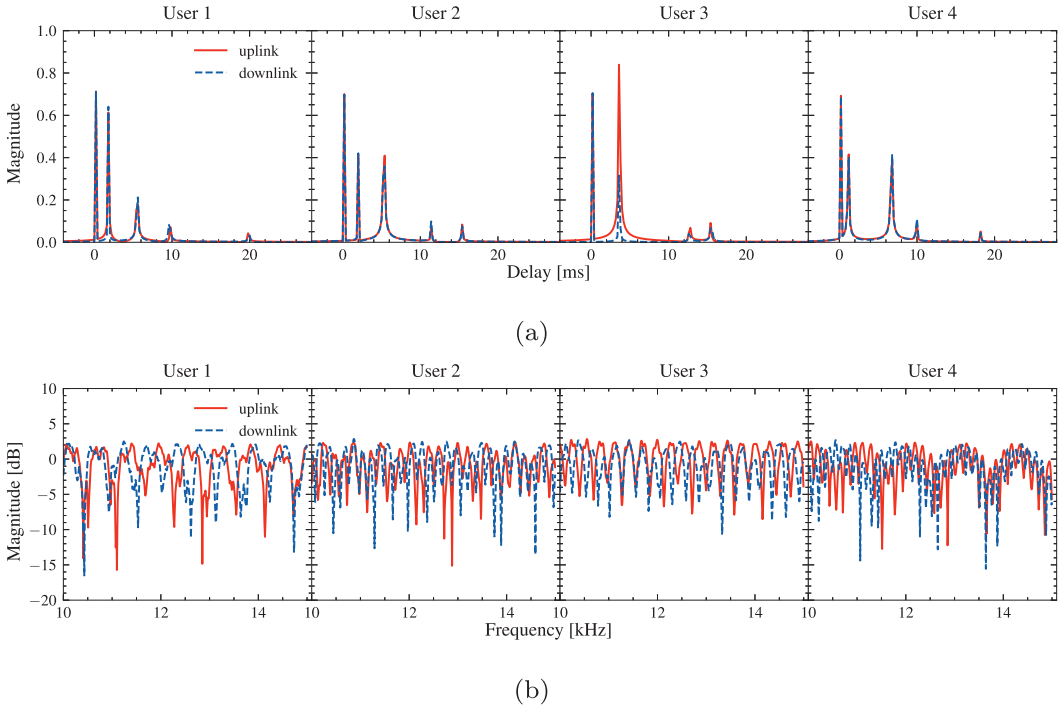

Fig. 2. (a) Impulse responses of the channel as seen on the uplink and downlink. (b) Channel transfer functions on the uplink and downlink.

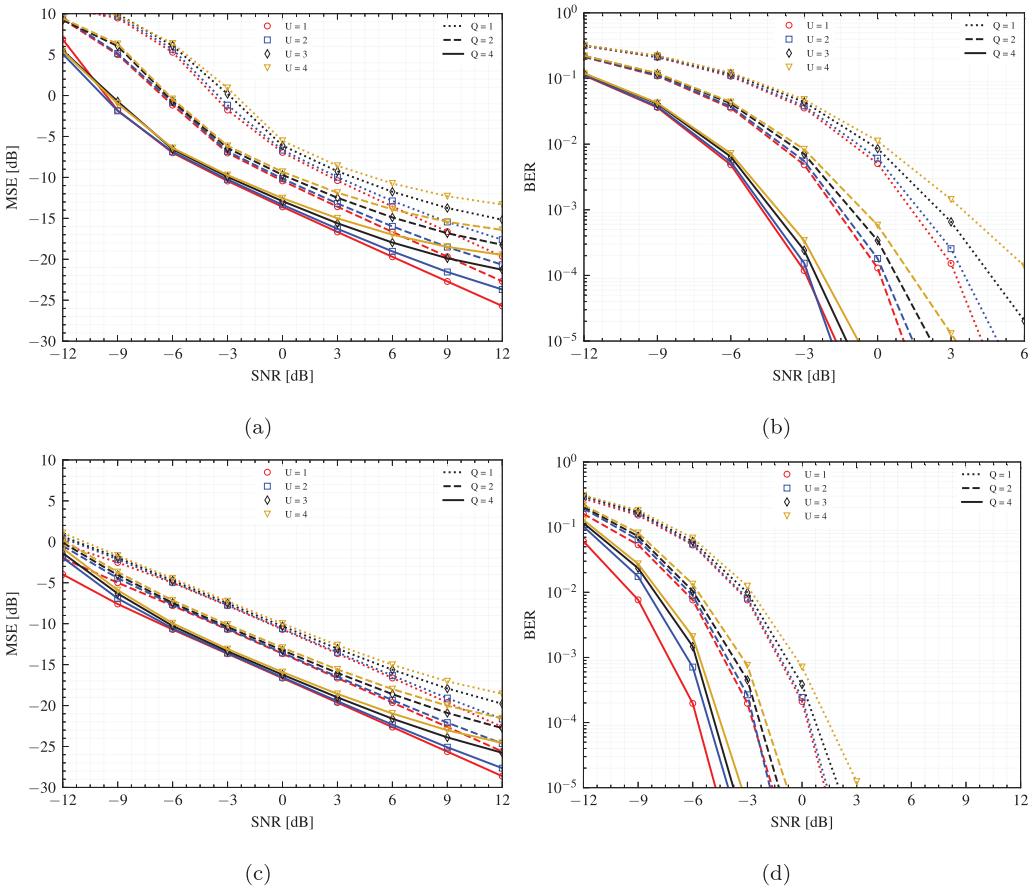

Fig. 3. System performance of principal path (top row) and multipath recombining (bottom row) techniques for uplink beamforming. The number of users is $U = 1$, 2, 3 or 4 and the spreading gain is $Q = 1$, 2 or 4. The modulation is differential QPSK.

power control mechanism) in such a way that the uplink and downlink channels of the users are normalized according to

$$\frac{1}{KM}\sum_{m=0}^{M-1}\sum_{k=0}^{K-1}\mathbb{E}\left\{|H_{k,u}^{m}|^2\right\}=1,\quad u=1,2,\ldots,U \tag{36}$$

Several possible channel impulse responses on the uplink and the downlink, as seen within the system bandwidth, are shown in Fig. 2(a). The channels have $P_u = 5$ significant paths and the total multipath spread of the channel is approximately 20 ms. The gains and delays are calculated from the channel geometry. The channel frequency responses, shown in Fig. 2(b), depict pronounced selectivity, and the discrepancy between the uplink and the downlink channels is remarkable.

5.1. Performance analysis: uplink

In the uplink, we consider the following beamforming approaches:

1. Principal path (PP): The beamforming weights are computed using the principal path angles of the users, which are estimated using (7).
2. Multipath recombining (MR): The beamforming weights are computed using the three strongest path angles of each user. These angles are estimated using (7).

The performance results are summarized in terms of data detection mean squared error (MSE) and bit error rate (BER) as functions of the input SNR ranging from −12 to 12 dB. Differentially coherent QPSK is implemented at the receiving side, and the data detection MSE is computed as

$$\text{MSE}=\frac{1}{N_r}\frac{1}{U}\frac{1}{I-1}\sum_{j=1}^{N_r}\sum_{u=1}^{U}\sum_{i=1}^{I-1}|b_{i,u}(j)-\hat{b}_{i,u}(j)|^2 \tag{37}$$

where $\hat{b}_{i,u}(j)$ is the estimate of the ith data symbol $b_{i,u}(j)$ of the uth user in the jth block. Each OFDM block contains an independent channel and noise realization, and $N_r = 100{,}000$ is the total number of realizations.

Fig. 3(a) shows the data detection MSE performance of principal path beamforming in the uplink. As one could expect, the MSE improves as the coding gain Q increases. Specifically, there is a 4 dB improvement in MSE when the Q doubles for the range of input SNR shown. In contrast, when the number of users increases (up to 4 users), the MSE degrades by approximately 4 dB to 6 dB for SNRs of 9 dB and 12 dB, respectively, and for $Q = 1, 2, 4$. However, this degradation is smaller at lower SNRs (SNRs less than 0 dB). This situation is alleviated when the base station steers beams to multiple propagation paths and the signal components are further recombined for data detection. Multipath recombining system performance is shown in Fig. 3(c). When the number of users increases and for all coding gains Q shown, the MSE degrades by 3.5 dB to 4.5 dB at SNRs of 9 dB and 12 dB, respectively. In addition, we observe that multipath recombining offers approximately a 3 dB improvement in MSE compared to principal path beamforming for all cases shown in Figs. 3(a) and 3(c).

Figs. 3(b) and 3(d) depict the BER performance results for principal path and multipath recombining for uplink beamforming. Each point of the plots is obtained by averaging over individual users' BERs. Fig. 3(b) illustrates that without coding, four users can be supported with BER of 1.75×10^{-3} at 3 dB of input SNR. This BER improves to 1.4×10^{-5} when the coding gain Q doubles. Additionally, we observe that for every doubling of Q, the SNR required to achieve the same performance is reduced by approximately 3 dB.

5.2. Performance analysis: downlink

The downlink multi-user communication technique consist of beamforming in the principal path directions of the users. The data detection

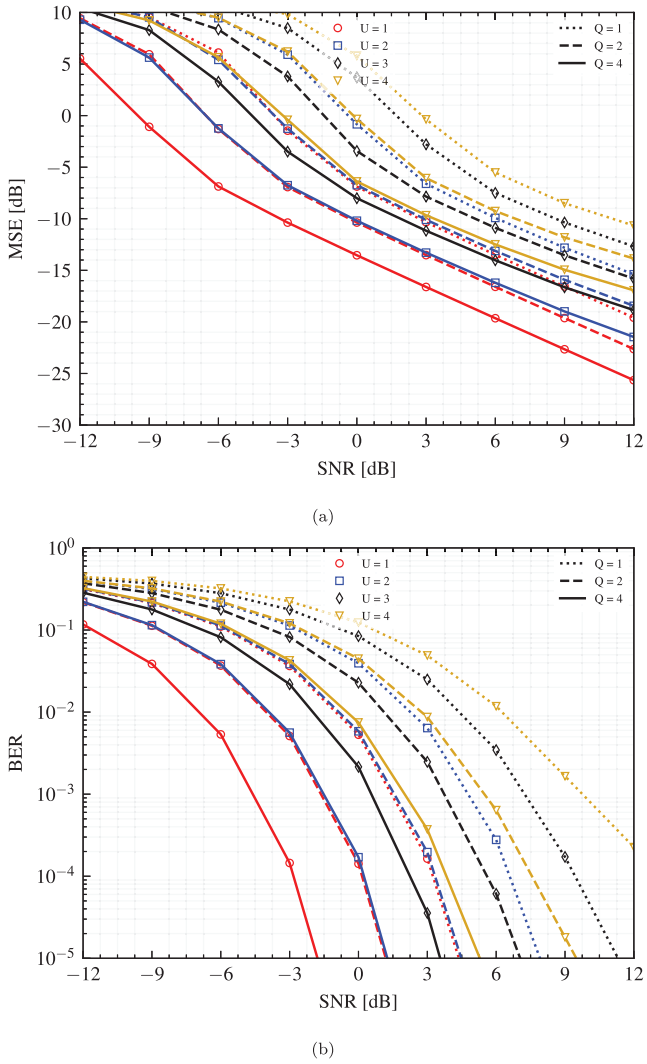

Fig. 4. System performance of principal path downlink beamforming. The number of users is $U = 1$, 2, 3 or 4 and the spreading gain is $Q = 1$, 2 or 4. The modulation is differential QPSK.

MSE on the downlink is illustrated in Fig. 4(a). As expected, the performance is bounded by that one of single user, i.e. $U = 1$ (no co-user interference), and coding gain $Q = 4$, which provides the lowest MSE in data detection. In contrast, the case that consists of $U = 4$ users (maximal co-user interference) and coding gain $Q = 1$, yields the highest MSE. There is 10 dB in MSE difference between these two cases. Similarly, it is observed that doubling the coding gain Q provides 3 dB extra of MSE.

The BER results show similar trends, as observed in Fig. 4(b). Without coding, four users can be supported with BER of 2×10^{-3} at 9 dB of input SNR. If the coding gain Q increases and the BER is kept constant, we observe that the required input SNR is reduced by 4.5 dB. In general, increasing the coding gain Q at a given SNR allows the support of more users and/or yields a lower BER.

Additionally, we analyze the performance of the principal path downlink beamforming for different multipath structures. At the onset of uplink transmission, the users are located at (ℓ_u, h_u), and during the downlink transmission the users drift uniformly at random speed $|\mathbf{v}_u| \sim \mathcal{U}[0, \text{v}]$ and random direction $\phi_u \sim \mathcal{U}[-\pi, \pi]$, for v = 1 m/s and 2 m/s, and $u = 1, 2, 3, 4$. The top row of Fig. 5 depicts the random locations of the users during the uplink–downlink cycle for v = 1 m/s and v = 2 m/s. Similarly, the bottom row of Fig. 5 illustrates the BER

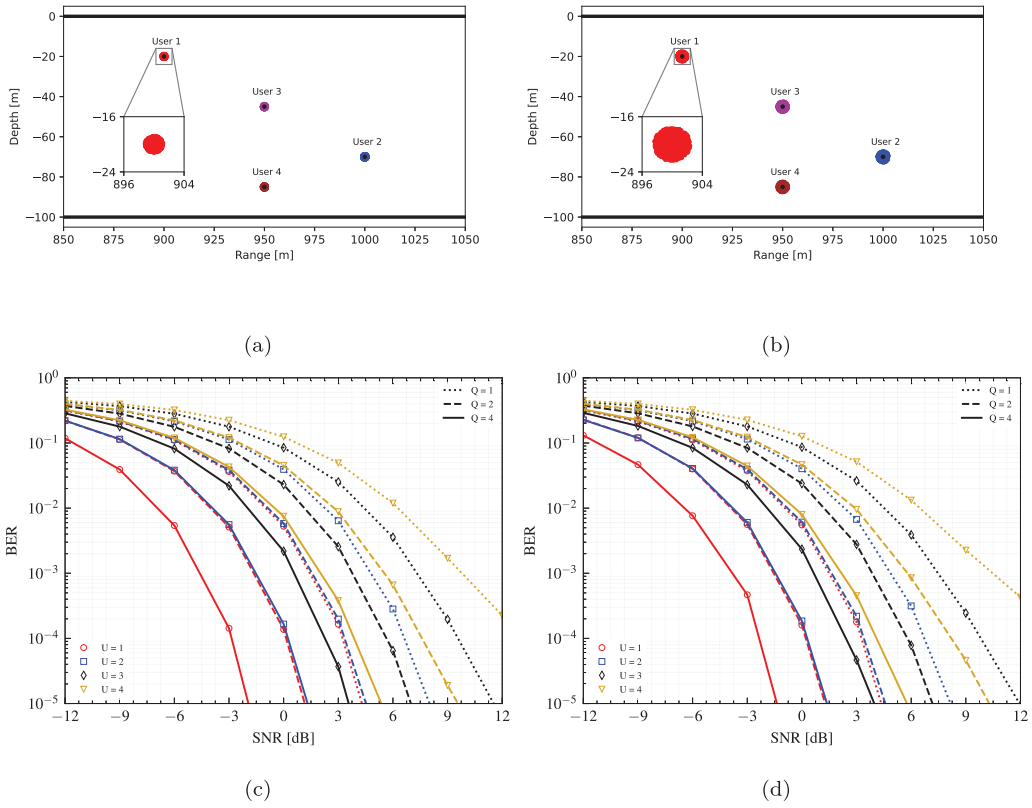

Fig. 5. The users drift randomly at the speed $|\mathbf{v}| \sim \mathcal{U}[0, \mathrm{v}]$ and direction $\phi_u \sim \mathcal{U}[-\pi, \pi]$ for (a) v = 1 m/s and (b) v = 2 m/s, and $u = 1, 2, 3, 4$. The bottom row (c)–(d) shows the corresponding system performance of principal path downlink beamforming. The number of users is U = 1, 2, 3 or 4 and the spreading gain is Q = 1, 2 or 4. The modulation is differential QPSK.

performance of the system, which slightly varies with respect to Fig. 4, even when the users drift at random speeds and directions.

6. Experimental results

We demonstrate the proposed system using the Acoustic Communications Testbed [24]. In a $U = 3$ multi-user setting, each user is equipped with a transmitter, while the BS is equipped with a 12-element array. The element spacing is $d = 5$ cm. The distance between the base station and the users are 3 m. The setup, including the base station and the remote users, are shown in Fig. 6. The signals used in the over-the-air experiments were of a cyclic prefix OFDM type, with initial carrier frequency $f_0 = 5$ kHz, bandwidth $B = 3$ kHz, and $K = 1024$ carriers. The guard interval is 32 ms. The modulation is QPSK with differential encoding. A 511-bit Gold sequence is used for front-end time synchronization, with a different sequence assigned to each user.

The uplink system performance is summarized in Fig. 7. The received SNR is around 20 dB, and each user's channel contains two paths. As we can observe from the plots, beamforming, null-steering and multipath recombining suppress the multi-user interference, providing good performance. For each user, there are two beampatterns shown, one for each of the propagation paths. Each pattern clearly points to a single maximum (the desired arrival), while three nulls are placed, one in the direction of the other multipath arrival, and two in the directions of two paths of the interfering user.

Once isolated through beamforming, the two multipath arrivals are combined to extract the full multipath gain. As expected, the performance improves as the spreading gain Q increases, again by 3 dB for every doubling of Q. This improvement of course comes at the price of a reduced information throughput. Specifically, with $Q = 1$, each user transmits in full band at 5.5 kbps, while for $Q = 2$ and 4, the per-user bit rate is 2.8 kbps and 1.4 kbps, respectively. In comparison, if pure DS-OFDM [19] were used, the spreading gain would have been required to stay above $\lceil BT_{mp} \rceil = 10$, and the corresponding throughput would have been much lower. Applying beamforming in conjunction with spreading, i.e. combining SDMA with CDMA, provides good performance at a much lower cost in throughput reduction.

In Fig. 8, we demonstrate the downlink performance. As expected, the performance improves as the spreading gain Q increases, following the same trend as before. One of the main benefits of the proposed system lies in its computational complexity. The users are required to perform minimal operations, while the heavy-lifting tasks of beamforming is performed on the BS side.

7. Conclusions

We introduced a multi-user multi-carrier communication network that utilizes a combined space-code division multiple access approach for both the uplink and downlink. The system incorporates broadband acoustic beamforming with null steering in the presence of interference, enabling the isolation of useful multipath components for subsequent multipath recombination. To evaluate the system's performance, we conducted simulations using a shallow water channel model and performed over-the-air acoustic transmissions. The results demonstrate the system's ability to accurately identify and isolate multiple propagation paths for each desired user while effectively suppressing multi-user interference. By combining coding techniques with broadband acoustic beamforming, we achieved excellent performance in terms of BER, as evidenced by both simulation and over-the-air tests. Notably, the combined space-code division multiple access approach relaxes the constraints typically imposed on spreading gain, leading to increased information throughput within the network.

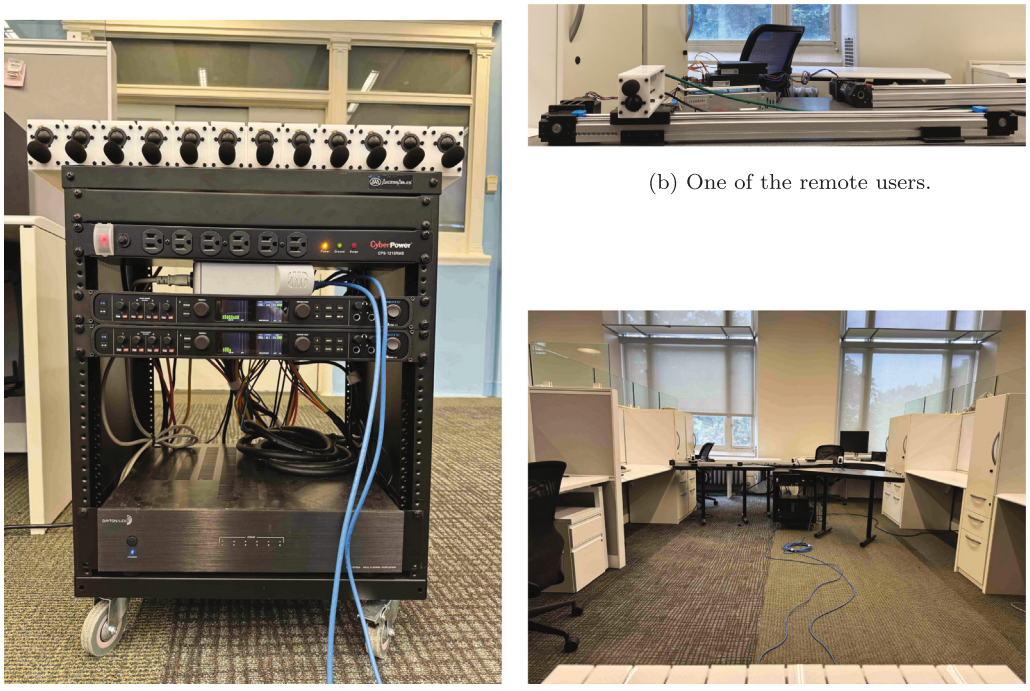

(a) Base station.

(b) One of the remote users.

(c) Experiment Setup.

Fig. 6. The acoustic communications testbed [24] setup.

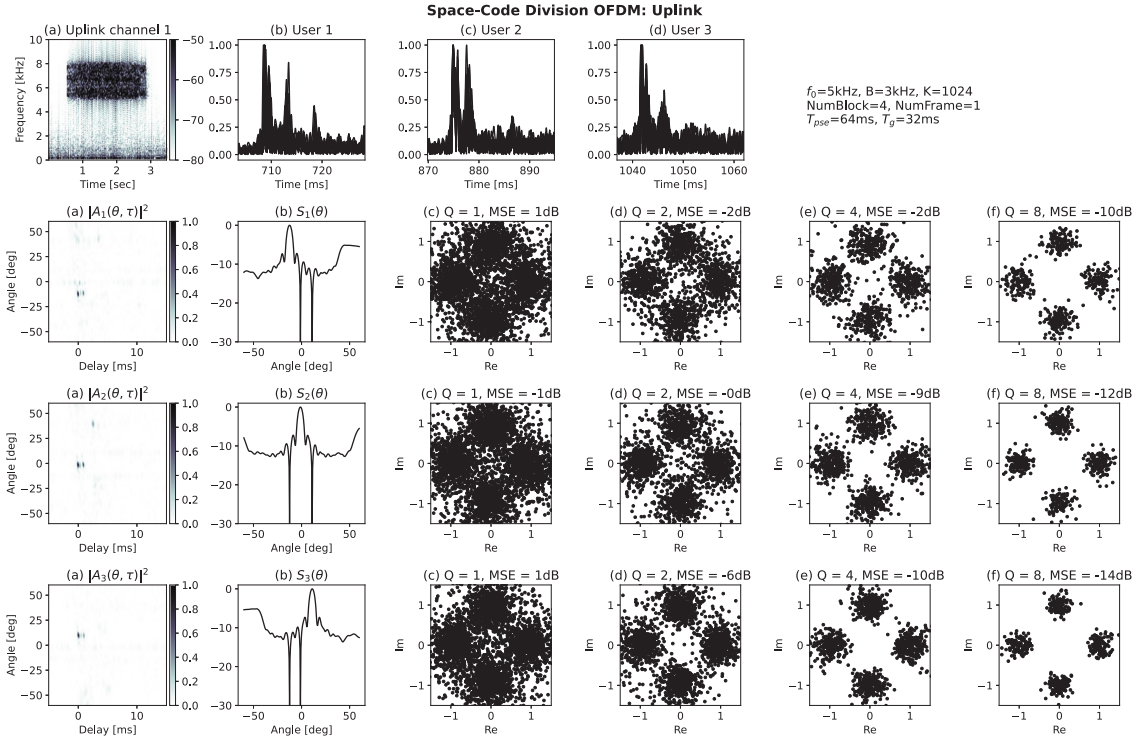

Fig. 7. Results of the uplink over-the-air transmission. QPSK OFDM signals were transmitted in 3 kHz of bandwidth using 1024 carriers. In this setup, there were three users ($U = 3$) and the BS was equipped with a 12-element horizontal array. In the first row, the spectrogram of the received signal, the cross-correlations between the users' preambles and the received signal, and the system parameters are shown. The second to last row correspond to user 1–3, respectively. Shown in each row are the $A(\theta, \tau)$ metric, the beampattern, the scatter plots of the estimated data symbols, with and without spreading.

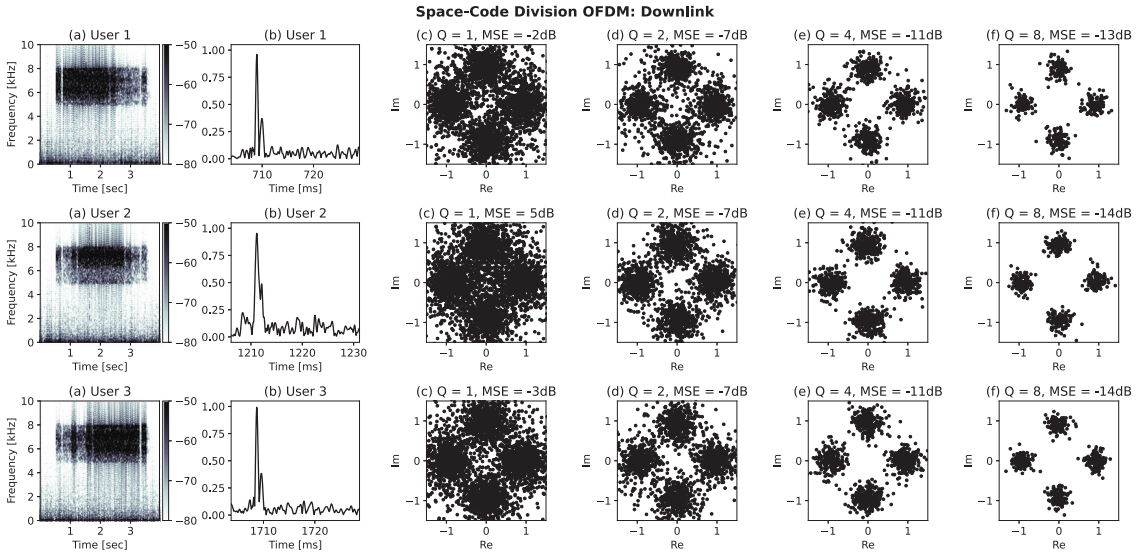

Fig. 8. Results of the downlink over-the-air transmission. QPSK OFDM signals were transmitted in 3 kHz of bandwidth using 1024 carriers. Shown in each row are spectrogram of the received signal, the cross-correlations between the users' preambles and their received signals, and the scatter plots of the estimated data symbols, with spreading code length of $Q = 1, 2, 4$ and 8.

CRediT authorship contribution statement

Zhengnan Li: Conceptualization, Data curation, Investigation, Methodology, Software, Visualization, Writing – original draft, Writing – review & editing. **Diego A. Cuji:** Conceptualization, Data curation, Investigation, Methodology, Software, Validation, Visualization, Writing – original draft, Writing – review & editing. **Milica Stojanovic:** Conceptualization, Funding acquisition, Investigation, Methodology, Project administration, Resources, Supervision, Validation, Writing – review & editing.

Declaration of competing interest

The authors declare that they have no known competing financial interests or personal relationships that could have appeared to influence the work reported in this paper.

Data availability

Data will be made available on request.

Acknowledgment

This work was supported by the Office of Naval Research under Grant N00014-20-1-2453.

References

[1] A. Song, M. Stojanovic, M. Chitre, Editorial underwater acoustic communications: Where we stand and what is next? IEEE J. Ocean. Eng. 44 (1) (2019) 1–6, http://dx.doi.org/10.1109/JOE.2018.2883872.

[2] E. Björnson, M. Bengtsson, B. Ottersten, Optimal multiuser transmit beamforming: A difficult problem with a simple solution structure [lecture notes], IEEE Signal Process. Mag. 31 (4) (2014) 142–148, http://dx.doi.org/10.1109/MSP.2014.2312183.

[3] G. Edelmann, T. Akal, W. Hodgkiss, S. Kim, W. Kuperman, H.C. Song, An initial demonstration of underwater acoustic communication using time reversal, IEEE J. Ocean. Eng. 27 (3) (2002) 602–609, http://dx.doi.org/10.1109/JOE.2002.1040942.

[4] M. Stojanovic, Retrofocusing techniques for high rate acoustic communications, J. Acoust. Soc. Am. 117 (3) (2005) 1173–1185, http://dx.doi.org/10.1121/1.1856411.

[5] G. Edelmann, H. Song, S. Kim, W. Hodgkiss, W. Kuperman, T. Akal, Underwater acoustic communications using time reversal, IEEE J. Ocean. Eng. 30 (4) (2005) 852–864, http://dx.doi.org/10.1109/JOE.2005.862137.

[6] H.C. Song, W.S. Hodgkiss, W.A. Kuperman, W.J. Higley, K. Raghukumar, T. Akal, M. Stevenson, Spatial diversity in passive time reversal communications, J. Acoust. Soc. Am. 120 (4) (2006) 2067–2076, http://dx.doi.org/10.1121/1.2338286.

[7] H.-C. Song, An overview of underwater time-reversal communication, IEEE J. Ocean. Eng. 41 (3) (2016) 644–655, http://dx.doi.org/10.1109/JOE.2015.2461712.

[8] T. Shimura, Y. Kida, M. Deguchi, Y. Watanabe, Y. Maeda, High-rate underwater acoustic communication at over 600 kbps × km for vertical uplink data transmission on a full-depth lander system, in: 2021 Fifth Underwater Communications and Networking Conference (UComms), 2021, pp. 1–4, http://dx.doi.org/10.1109/UComms50339.2021.9598067.

[9] Y. Kida, M. Deguchi, Y. Watanabe, T. Shimura, Experiments for long-range high-rate underwater acoustic MIMO communication using adaptive passive time reversal, in: 2023 IEEE Underwater Technology, UT, 2023, pp. 1–6, http://dx.doi.org/10.1109/UT49729.2023.10103409.

[10] D. Kilfoyle, J. Preisig, A. Baggeroer, Spatial modulation experiments in the underwater acoustic channel, IEEE J. Ocean. Eng. 30 (2) (2005) 406–415, http://dx.doi.org/10.1109/JOE.2004.834168.

[11] T.C. Yang, A study of spatial processing gain in underwater acoustic communications, IEEE J. Ocean. Eng. 32 (3) (2007) 689–709, http://dx.doi.org/10.1109/JOE.2007.897072.

[12] C. He, J. Huang, Z. Ding, A variable-rate spread-spectrum system for underwater acoustic communications, IEEE J. Ocean. Eng. 34 (4) (2009) 624–633, http://dx.doi.org/10.1109/JOE.2009.2030222.

[13] N. Iruthayanathan, K.S. Vishvaksenan, V. Rajendran, Performance of spread spectrum based multi-carrier system in underwater communication using transmitter pre-processing, IEEE Access 4 (2016) 5128–5134, http://dx.doi.org/10.1109/ACCESS.2016.2591587.

[14] P. van Walree, E. Sangfelt, G. Leus, Multicarrier spread spectrum for covert acoustic communications, in: Proceedings of OCEANS 2008, 2008, pp. 1–8, http://dx.doi.org/10.1109/OCEANS.2008.5151841.

[15] G. Leus, P. van Walree, Multiband OFDM for covert acoustic communications, IEEE J. Sel. Areas Commun. 26 (9) (2008) 1662–1673, http://dx.doi.org/10.1109/JSAC.2008.081206.

[16] D. Egnor, L. Cazzanti, J. Hsieh, G.S. Edelson, Underwater acoustic single- and multi-user differential frequency hopping communications, in: OCEANS 2008, 2008, pp. 1–6, http://dx.doi.org/10.1109/OCEANS.2008.5152011.

[17] D.A. Cuji, Z. Li, M. Stojanovic, Multi-user communications for acoustic OFDM: A broadband beamforming approach, in: 2022 Sixth Underwater Communications and Networking Conference, UComms, 2022, pp. 1–4, http://dx.doi.org/10.1109/UComms56954.2022.9905699.

[18] D.A. Cuji, M. Stojanovic, Transmit beamforming for underwater acoustic OFDM systems, IEEE J. Ocean. Eng. (2023) 1–18, http://dx.doi.org/10.1109/JOE.2023.3295474.

[19] Z. Li, M. Stojanovic, Multicarrier acoustic communications in multiuser and interference-limited regimes, IEEE J. Ocean. Eng. 48 (2) (2023) 542–553, http://dx.doi.org/10.1109/JOE.2022.3212826.

[20] Z. Li, D.A. Cuji, M. Stojanovic, Combined code division and space division multiple access for broadband acoustic networks, in: Proceedings of the 16th

International Conference on Underwater Networks & Systems, WUWNet '22, Association for Computing Machinery, New York, NY, USA, 2022, pp. 1–6, http://dx.doi.org/10.1145/3567600.3568145.

[21] P. Qarabaqi, M. Stojanovic, Statistical characterization and computationally efficient modeling of a class of underwater acoustic communication channels, IEEE J. Ocean. Eng. 38 (4) (2013) 701–717, http://dx.doi.org/10.1109/JOE.2013.2278787.

[22] Z. Li, D.A. Cuji, M. Stojanovic, A joint angle and delay detection scheme using OFDM over broadband acoustic links, in: 2022 IEEE International Symposium on Phased Array Systems & Technology, PAST, 2022, pp. 01–05, http://dx.doi.org/10.1109/PAST49659.2022.9974993.

[23] B. Friedlander, B. Porat, Performance analysis of a null-steering algorithm based on direction-of-arrival estimation, IEEE Trans. Acoust. Speech Signal Process. 37 (4) (1989) 461–466, http://dx.doi.org/10.1109/29.17526.

[24] D.A. Cuji, Z. Li, M. Stojanovic, ACT: an acoustic communications testbed, in: IEEE INFOCOM 2022 - IEEE Conference on Computer Communications Workshops, INFOCOM WKSHPS, IEEE, 2022, pp. 1–6, http://dx.doi.org/10.1109/INFOCOMWKSHPS54753.2022.9798284.

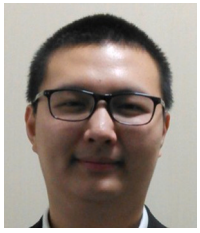

Zhengnan Li received the B.S. degree in communication engineering from Shandong University of Technology, Zibo, China, in 2016, and the M.S. degree in electrical engineering from Northeastern University, Boston, MA, USA, in 2018; where he is currently working towards his Ph.D. degree in electrical engineering.

His research interests include statistical signal processing and digital communications, and their applications to underwater acoustic systems.

Email address: li.zhengn@northeastern.edu

Diego A. Cuji received the B.S. degree in electronic engineering from Universidad Politecnica Salesiana, Cuenca, Ecuador, in 2014 and the M.S. degree in electrical and computer engineering in 2019 from Northeastern University, Boston, MA, USA, where he is currently working toward the Ph.D. degree in electrical engineering.

His research interests include digital communications, OFDM, beamforming, and underwater acoustic communications.

Email address: cujidutan.d@northeastern.edu

Milica Stojanovic graduated from the University of Belgrade, Serbia, in 1988, and received M.S. (1991) and Ph.D. (1993) degrees in electrical engineering from Northeastern University, Boston, Massachusetts. She was a Principal Scientist at MIT, and in 2008 joined Northeastern University, where she is currently a Professor of electrical and computer engineering. She is also a Guest Investigator at the Woods Hole Oceanographic Institution.

Her research interests include digital communications theory, statistical signal processing and wireless networks, and their applications to underwater acoustic systems.

Milica is an Associate Editor for the IEEE Journal of Oceanic Engineering, and a past Associate Editor for the IEEE Transactions on Signal Processing and the IEEE Transactions on Vehicular Technology. She chairs the IEEE Ocean Engineering Society (OES) Technical Committee for Underwater Communication, Navigation and Positioning, and serves on the Editorial Board of the IEEE Signal Processing Magazine. She is an IEEE Fellow (2010), the recipient of the 2015 IEEE/OES Distinguished Technical Achievement Award, and the 2018 IEEE/OES Distinguished Lecturer.

Email address: millitsa@ece.neu.edu